Journal of Hazardous Materials 501 (2026) 140677

Contents lists available at ScienceDirect

Journal of Hazardous Materials

journal homepage: www.elsevier.com/locate/jhazmat

A portable microfluidic platform for on-site detection of *Aeromonas hydrophila* in aquaculture water using multi-enzyme isothermal rapid amplification

Zhuangzhuang Bai [a,b,c], Yanying Zhang [f], Chen Li [e], Jie Han [a,b,c], Tonglei Wu [f], Cong Wang [a,b,c], Yan Zhang [d,*], Daoliang Li [a,b,c,**]

[a] National Innovation Center for Digital Fishery, China Agricultural University, Beijing 100083, China
[b] MARA Key Laboratory of Smart Farming Technologies for Aquatic Animal and Livestock, College of Information and Electrical Engineering, China Agricultural University, Beijing 100083, China
[c] Beijing Engineering and Technology Research Centre for Internet of Things in Agriculture, China Agriculture University, Beijing 100083, China
[d] MARA Key Laboratory of Pest Monitoring and Green Management, College of Plant Protection, China Agricultural University, Beijing 100193, China
[e] College of Physics Science and Technology, Hebei Normal University of Science and Technology, Qinhuangdao, 066004, China
[f] Hebei Provincial Key Laboratory of Preventive Veterinary Medicine, Hebei Normal University of Science and Technology, Qinhuangdao 066004, China

HIGHLIGHTS

- Portable microfluidic platform for on-site detection of *A. hydrophila* in aquaculture water.
- Integrates nucleic acid extraction, precise pipetting, amplification, and detection.
- Achieves detection within 40 min with LOD of 10 CFU·mL^{-1}.
- Enables multiplex pathogen detection via interchangeable primers and probes.
- Miniature vibration motor and PID heating ensure temperature and reaction uniformity.

GRAPHICAL ABSTRACT

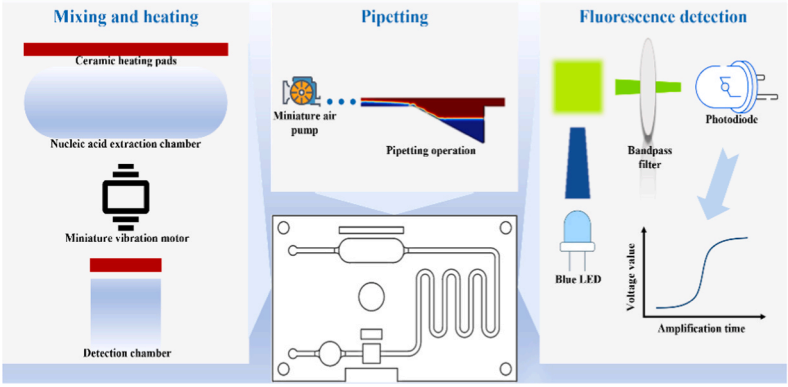

ARTICLE INFO

Keywords:
Aeromonas hydrophila
Portable microfluidic platform
Multi-enzyme isothermal rapid amplification
Aquaculture water
On-site detection

ABSTRACT

Aeromonas hydrophila is a significant pathogenic bacterium in aquaculture, causing severe diseases in farmed animals and resulting in substantial economic losses. To enable rapid on-site detection, we developed a portable microfluidic platform that integrates multi-enzyme isothermal rapid amplification (MIRA) with automated fluid handling. The chip design incorporated a miniature vibration motor and ceramic heating pads to maintain precise temperature control and ensure reaction homogeneity throughout nucleic acid extraction and amplification. A miniature air pump drove the crude DNA extract through the chip in a single pipetting step for accurate quantification. The extracted DNA was subsequently transferred to a reaction chamber preloaded with MIRA

* Correspondence to: College of Plant Protection, China Agricultural University, 2 Yuanmingyuan West Road, Beijing 100193, China.
** Correspondence to: China Agricultural University, P. O. Box 121, 17 Tsinghua East Road, Beijing 100083, China.
E-mail addresses: yzhang@cau.edu.cn (Y. Zhang), dliangl@cau.edu.cn (D. Li).

https://doi.org/10.1016/j.jhazmat.2025.140677
Received 19 August 2025; Received in revised form 11 November 2025; Accepted 30 November 2025
Available online 1 December 2025

reagents for isothermal amplification at 39 °C under real-time fluorescence monitoring. This platform detected *A. hydrophila* in water samples within 40 min, achieving a linear range from 1×10^2 to 1×10^7 CFU·mL^{-1} and a limit of detection (LOD) of 10 CFU·mL^{-1}. Notably, its modular design allows easy interchange of primers and probes, making the platform readily adaptable for detecting diverse bacterial pathogens in aquaculture.

1. Introduction

The intensification of aquaculture has driven continuous growth in global production, establishing it as a primary source of aquatic products [1–3]. However, high-density farming practices have increased the incidence of diseases caused by bacteria, fungi, viruses, and parasites, adversely affecting global aquaculture production and impeding its sustainable development [4,5]. Among these threats, bacterial diseases are particularly detrimental to aquaculture sustainability due to their diverse pathogenicity, broad host range, high infectivity, rapid transmission, and remarkable environmental adaptability [6].

Aeromonas species are highly pathogenic to numerous aquatic animals among bacterial pathogens [7]. They cause Motile Aeromonas Septicemia (MAS), a disease associated with substantial economic losses in aquaculture [8]. Regional epidemiological studies have consistently identified *A. hydrophila* as the predominant pathogen responsible for MAS outbreaks [9–12]. This pathogen is widely distributed in aquatic environments and threatens a broad spectrum of hosts, including fish [13], crustaceans [14,15], and amphibians [16]. Its significant pathogenicity is largely attributed to diverse virulence factors, such as aerolysin, hemolysins, and proteases [17]. The aerolysin toxin, encoded by the *aerA* gene, is a major contributor to high-mortality outbreaks [18]. Owing to its prevalence in pathogenic strains and critical role in pathogenesis, the *aerA* gene serves as an ideal target for specific molecular detection.

A waterborne challenge model simulating natural MAS occurrence demonstrated that under controlled conditions, *A. hydrophila* concentrations exceeding 10^5 CFU·mL^{-1} significantly increase mortality rates in channel catfish [19]. However, in actual aquaculture environments, factors such as water temperature fluctuations, host immune status, and co-infections can substantially increase outbreak risks even at lower bacterial concentrations [20]. Moreover, the minimum infectious dose required to trigger outbreaks across different farming systems remains unclear. Therefore, routine and accurate quantification of *A. hydrophila* in aquaculture water is essential. This enables a shift from reactive treatment to proactive risk management, which is critical for ensuring production security, guiding science-based control strategies, and preventing substantial economic losses [21–23].

Currently, polymerase chain reaction (PCR) and real-time quantitative PCR (qPCR) are considered the gold standard for molecular diagnosis in laboratory settings, offering superior detection speed, sensitivity, and specificity compared to conventional bacteriological methods [24]. However, these methods require sophisticated equipment, trained personnel, and time-intensive procedures, limiting their practicality for rapid on-site diagnosis in aquaculture operations [25]. With advances in molecular biology, isothermal nucleic acid amplification (ITA) technologies such as MIRA, loop-mediated isothermal amplification (LAMP), rolling circle amplification (RCA), and hybridization chain reaction (HCR) have emerged as viable alternatives to conventional PCR [26]. These methods enable highly efficient nucleic acid amplification at a constant temperature, eliminating the need for thermal cyclers [27]. Among them, MIRA has attracted considerable interest due to its rapid reaction time, simple temperature requirements, and ease of primer and probe design [28,29]. Despite MIRA's inherent potential for field deployment, translating this capability into practical on-site diagnostic tools remains challenging. Current detection systems typically rely on discrete modules for nucleic acid extraction, amplification, and detection, involving multiple manual steps and reagent transfers. This leads to operational complexity, high contamination risk, and considerable demand for operator expertise, collectively hindering reliability and practicality in real-world aquaculture settings [30]. Therefore, integrating all detection steps into a single microfluidic chip represents an ideal solution [31–33].

Microfluidic chips, often termed "lab-on-a-chip" systems, provide a promising platform for deploying ITA in field settings [34]. Leveraging advantages such as miniaturization, integration, and automation, these systems effectively overcome limitations of conventional molecular diagnostics, including operational complexity and reliance on specialized equipment [35]. In recent years, researchers have increasingly focused on developing efficient and reliable integrated systems to address on-site detection challenges in resource-limited settings [36,37]. These efforts highlight that the systematic integration of different functional modules to achieve synergistic effects and enhance overall practicality represents a key pathway to overcoming application bottlenecks [38]. Notably, Li et al. [39] integrated recombinase polymerase amplification (RPA) on a centrifugal microfluidic chip, achieving multiplex detection of five high-risk bacterial pathogens in shrimp aquaculture. To automate the integration of ITA with CRISPR/Cas12a detection, Shu et al. [40] developed a spatially encoded centrifugal microfluidic chip that physically separates amplification and detection processes while incorporating dual-temperature zones to accommodate different ITA methodologies (RPA/LAMP) on a single platform. However, in these systems, DNA extraction was performed off-chip, limiting their practical utility for on-site detection. While previous studies have demonstrated the feasibility of on-chip integration of nucleic acid extraction, amplification, and detection, these systems often rely on sophisticated fluidic control mechanisms to achieve precise quantitative DNA template transfer [41,42]. A representative example is the digital microfluidic platform developed by Liao et al., which employs programmable electrode arrays and electrowetting-on-dielectric technology to generate and manipulate controlled-volume DNA droplets [43]. Nevertheless, such sophisticated fluidic control mechanisms significantly increase operational complexity and cost, underscoring the need for simpler and more practical integration strategies.

This study developed an integrated portable microfluidic platform incorporating nucleic acid extraction, isothermal amplification, microfluidic control, and electronic systems. The self-contained platform achieved quantitative detection of *A. hydrophila* in aquaculture water without ancillary equipment (Fig. 1). We innovatively fabricated a three-dimensional microfluidic chip that allows direct integration of a miniature vibration motor and ceramic heating pads. This design enables solution homogenization in both nucleic acid extraction and detection chambers using only a single vibration motor. Precise thermal regulation across all reaction zones is maintained by proportional-integral-derivative (PID)-controlled ceramic heaters. Furthermore, the on-chip pipetting area, comprising multiple solution retention zones, achieves one-step quantitative transfer of DNA template solution via pneumatic actuation. The transferred DNA template solution reacts with pre-loaded MIRA reagents in the detection chamber at 39 °C, enabling target quantification through real-time fluorescence monitoring.

2. Materials and methods

2.1. Experimental materials

A. hydrophila (ATCC7966), *A. veronii* (CL), *Pseudomonas aeruginosa* (ATCC27853), *Pseudomonas fluorescens* (CL), *Vibrio harveyi* (CL), *Vibrio parahaemolyticus* (CL), *Vibrio anguillarum* (CL), *Vibrio cholerae* (CL),

Vibrio alginolyticus (CL), *Streptococcus agalactiae* (CL), and *Streptococcus iniae* (CL) were provided by the Hebei Provincial Key Laboratory of Preventive Veterinary Medicine. *A. sobria* (QHD) was obtained from the Department of Aquatic Science, College of Marine Sciences, Hebei Agricultural University. Detailed information on the field strains of *A. hydrophila* (Ah-1, Ah-2, Ah-3, and Ah-4) is provided in the Supplementary Materials. The rapid nucleic acid release agent (DNA type) and rapid thermostatic amplification kit (fluorescent type) were purchased from Amp-Future Biotech Co., Ltd (Changzhou, China). Poly(dimethylsiloxane) (PDMS) from Dow Corning was used in the fabrication of microfluidic chips. Additional details can be found in the Supplementary Materials.

2.2. Bacterial culture and nucleic acid extraction

Bacterial strains were stored at −20 °C until use. For cultivation, 10 μL of bacterial suspension was inoculated into 1 mL of an appropriate liquid medium and incubated with shaking at 200 rpm overnight at their optimal temperature for each strain. Serial dilutions ranging from 1×10^1–1×10^8 CFU·mL^{-1} were prepared using sterile phosphate-buffered saline (PBS). Bacterial concentrations were determined by the plate count method, where 100 μL of each diluted suspension was spread onto solid medium and incubated overnight at the appropriate temperature. Colonies were enumerated the following day to calculate the bacterial concentration. Additional details are provided in the Supplementary Materials. For nucleic acid extraction, the bacterial suspension was mixed with a rapid nucleic acid release reagent (containing components LD-1 and LD-2) at a volume ratio of 25:4:1. The mixture was then incubated under optimal reaction conditions to obtain the crude bacterial DNA template.

2.3. Design and screening of primers and probe

The *aerA* gene is highly conserved and critical for the virulence of *A. hydrophila*, being present in most pathogenic isolates [18]. It was therefore selected as the target for molecular detection. To ensure

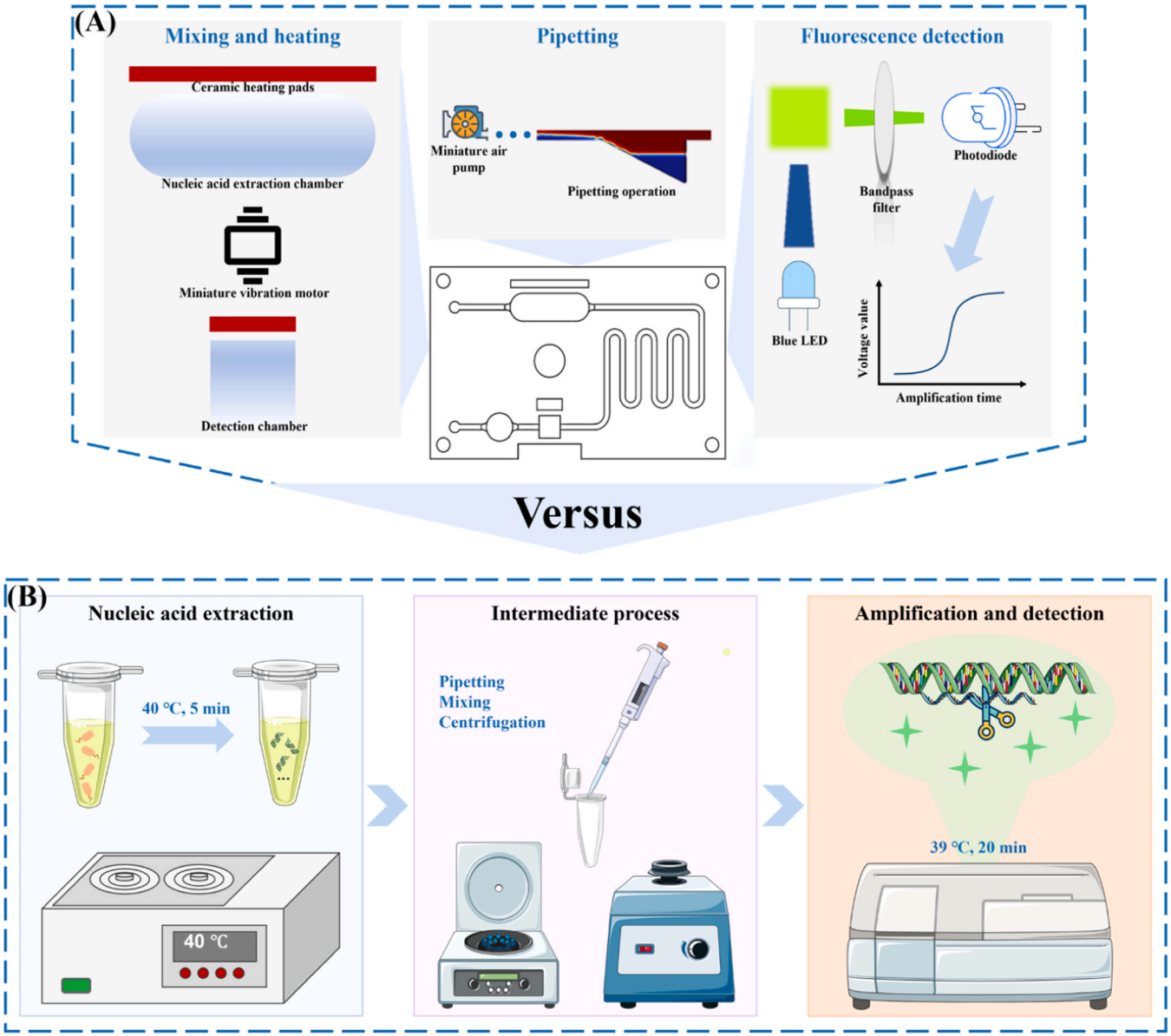

Fig. 1. Schematic comparison of the portable microfluidic platform and the conventional detection platform for *A. hydrophila*. (A) The portable microfluidic platform. The detection workflow on this platform integrates nucleic acid extraction, precise pipetting, amplification, and detection. (B) The conventional detection platform. The conventional laboratory-based workflow relies on sophisticated equipment, trained personnel, and time-intensive procedures.

detection specificity, the *aerA* gene sequence of *A. hydrophila* (Gene ID: 4490401) was compared with those of *A. veronii* (Gene ID: 60846399) and *A. sobria* (Gene ID: 58924504) using DNAman (Lynnon Biosoft, USA) software. As shown in Fig. S1, the nucleotide homology was 70.3 % with *A. veronii* and 69.88 % with *A. sobria*, which provided sufficient sequence divergence for the design of species-specific detection assays. Based on this comparison, three forward primers, three reverse primers, and one fluorescent probe targeting the *aerA* gene were designed online (https://ezassay.com/primer) (Table 1). To further validate specificity, Primer-BLAST was used to analyze all candidate sequences. All primers and the probe were synthesized by Sangon Biotech (Shanghai, China). Finally, the nine primer-probe sets were evaluated by in-tube MIRA assay using a real-time PCR system (FQD-96A, Bioer Technology, Hangzhou, China) to identify the optimal combination.

2.4. MIRA nucleic acid detection

The MIRA assay was performed in a 50 μL reaction system targeting the *aerA* gene of *A. hydrophila*. The reaction mixture consisted of 29.4 μL of buffer A, 2 μL of forward primer (10 μM), 2 μL of reverse primer (10 μM), 0.6 μL of fluorescent probe (10 μM), 13.5 μL of DNA template, and ddH_2O, with 2.5 μL of buffer B. After thorough mixing, the reactions were incubated at the optimal temperature for 20 min. Fluorescence signals were recorded at 30-second intervals throughout the amplification process. The fluorescence threshold was defined as the mean fluorescence of the first four cycles plus ten standard deviations, in accordance with established isothermal amplification quantification methods [44]. The time threshold, defined as the time required for the amplification curve to cross this predefined threshold, was found to correlate quantitatively with *A. hydrophila* concentrations, enabling the establishment of a standardized calibration curve. All experiments were performed with three independent replicates, each consisting of triplicate technical measurements.

2.5. Design and fabrication of the microfluidic chips

The microfluidic chip plays a critical role in enabling rapid on-site pathogen detection. As shown in Fig. 2 and Fig. S2, the chip (55 mm × 34 mm × 9.5 mm) features a two-layer architecture with four functional compartments: (1) a nucleic acid extraction chamber (~210 μL) containing bacterial samples and rapid nucleic acid release agents for crude DNA extraction; (2) a pipetting area (~175 μL) for quantitative transfer of DNA template while retaining excess sample; (3) a reagent storage chamber (~70 μL) pre-loaded with MIRA reaction reagents; and (4) a detection chamber (~70 μL) where isothermal amplification and real-time monitoring occur. The detection and reagent storage chambers were specifically engineered to accommodate both liquid and lyophilized reagent formats, ensuring compatibility with various commercial kits.

Table 1
Primer and probe sequences used in this study.

Primer/Probe name	Sequences (5'-3')
F1	GCCTGTTTTCACTGGGCCAGGAGGTATGTGG
F2	CCTGTTTTCACTGGGCCAGGAGGTATGTGG
F3	TCATATCCGGCCTGCTGATGGCACAGGCTC
R1	AATGAAATTCGCACTGTCGTGTACCAGTCGC
R2	TCTGGAATATCCAGGGCTGACAAGGTTGG
R3	TGGTTGGCTTAATGAAATTCGCACTGTCGTG
Probe	AAAAGCAATATTATCAATATGATGGGGCAGTG(FAM-dT)G(THF)C(BHQ1-dT)AAATAAGCGGTCTGGCCA[C3-spacer]

FAM: 6-Carboxyfluorescein; THF: tetrahydrofuran; BHQ1: black hole quencher 1.

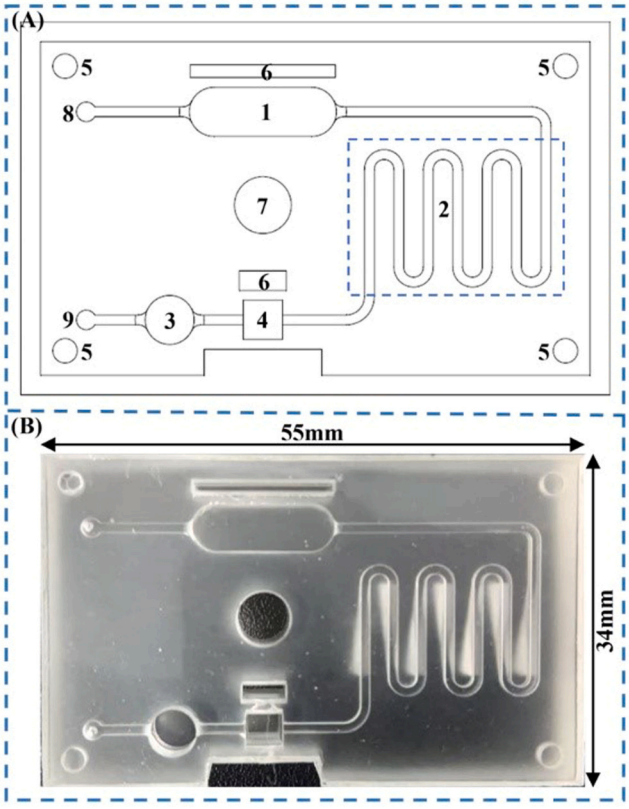

Fig. 2. Schematic diagram and photograph of the fabricated microfluidic chip. (A) Schematic illustration of the chip layout and key components. 1, Nucleic acid extraction chamber. 2, Pipetting area. 3, Reagent storage chamber. 4, Detection chamber. 5, Alignment hole. 6, Square perforation. 7, Circular perforation. 8, Sample inlet. 9, Air inlet. (B) Photograph of the microfluidic chip.

The chip incorporates three specialized perforated structures: one circular perforation housing a miniature vibration motor for efficient reagent mixing in both the extraction and detection chambers, and two square perforations containing ceramic heating pads for independent temperature control of the respective reaction zones.

Given the structural complexity of the designed chip, we employed a replica molding fabrication approach. First, the layered channel structures were designed using SolidWorks (Concord, MA). A high-precision mold was then fabricated via 3D printing (Micro P215 plus, Xingsheng Precision, China) (Fig. S3). Following the procedure outlined in Fig. S4, we successfully produced a three-dimensional microfluidic chip. Additional fabrication details are provided in the Supplementary Material.

2.6. Hydrophilic and hydrophobic modification of the microfluidic chips

Surface modification of the PDMS chip was performed to achieve precise fluid control. The pipetting area was rendered hydrophilic by filling its trenches with a treatment reagent diluted in isopropanol (7:3 v/v) for 1 min. The reagent was then removed, and the region was air-dried at room temperature. In contrast, the reaction chambers and connecting channels were made hydrophobic by uniformly coating them with a hydrophobic treatment reagent, followed by drying at ambient temperature. All modified chips were stored under vacuum at 4 °C prior to use.

2.7. Development of the supporting peripherals

The supporting peripherals are essential components for automated on-chip detection of *A. hydrophila*. As shown in Fig. S5, these devices are

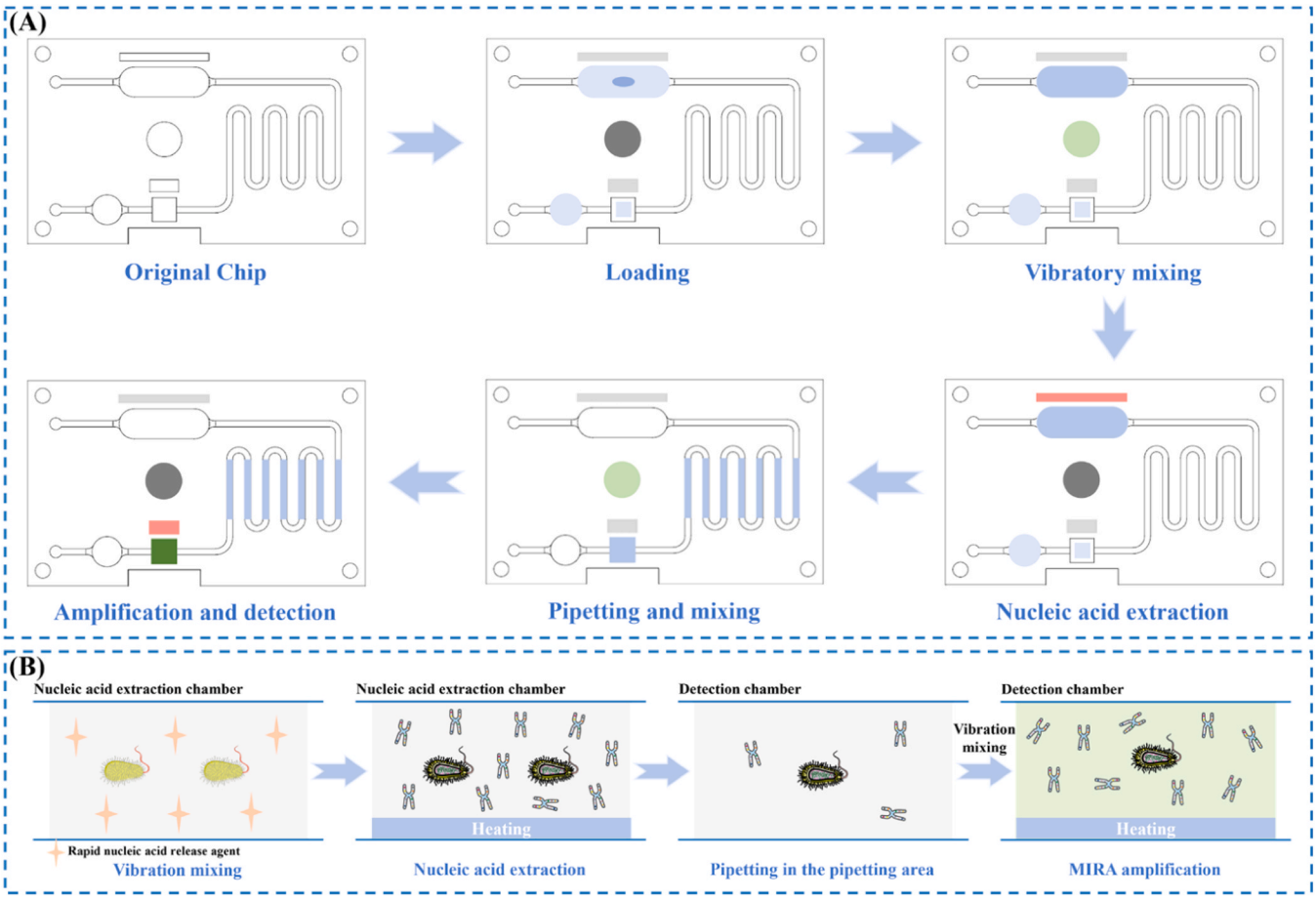

Fig. 3. Schematic illustration of the on-chip detection principle and workflow. (A) Operational workflow. Color changes in the circular and square perforations reflect the operational status of the vibration motor and heating pads, respectively. Efficient reagent mixing is shown by the color deepening in the extraction chamber, while a color shift in the detection chamber indicates the generation of positive fluorescent signals. (B) Detection principle. The change in nucleic acid molecule quantity reflects the successful completion of the precise pipetting and the MIRA amplification, respectively.

built around an STM32F103ZET6 microcontroller (STMicroelectronics, Geneva, Switzerland), which coordinates a miniature air pump (Weiye Machinery Manufacturing Co., Ltd., Taizhou, China) for precise fluid handling and a miniature vibration motor (TEJIATE, Shenzhen, China) for efficient reagent mixing. For nucleic acid amplification and real-time fluorescence monitoring, ceramic heating pads (Huameng New Materials, Guangzhou, China) with integrated temperature sensors (PT100, Heraeus, Germany) were installed in the chip's square perforations and programmed to maintain constant temperatures of 40 °C and 39 °C, respectively. A 470 nm blue light-emitting diode (LED) (L470–06, USHIO, Japan) was positioned beneath the detection chamber to excite the fluorescent probe, while a photodiode (S1223, Hamamatsu, Japan) equipped with a 525 nm bandpass filter (EM525/20, HB Optical Technology Co., Ltd., Shenyang, China) was aligned laterally to collect emitted fluorescence and minimize ambient light interference. Normalized voltage values were used to characterize changes in the fluorescent signal, calculated as the ratio of the measured voltage to the detection range (3.3 V) of the microcontroller's analog-to-digital converter. Signal processing and result generation were implemented through embedded C language software.

To ensure operational reliability in humid aquaculture environments, all components were housed in a waterproof enclosure fabricated from Acrylonitrile Butadiene Styrene (ABS) plastic (Yifeng Plastic Industry, Zhejiang, China) (Fig. S6). An internally printed partition (Bambu Lab X1, Shenzhen, China) physically separated the upper detection area from the underlying electronics. During operation, parameters were configured via a serial touchscreen (TJC4827T143_011C, TAOJINGCHI, Shenzhen, China) interface. Initiation of the "Start" command triggered the microcontroller to execute the fully automated testing protocol.

2.8. Detection of target bacteria on chip

Fig. 3 schematically illustrates the working principle and operational workflow of the microfluidic detection system for *A. hydrophila*. The detection process begins by loading the chip with the bacterial sample, rapid nucleic acid release agent, and MIRA amplification reagents (which can be pre-loaded and stored at −20 °C). Upon initiation, the integrated miniature vibration motor operates for 10 s to ensure thorough mixing of the reagents. The ceramic heating pad then maintains the nucleic acid extraction chamber at 40 °C for 5 min to facilitate DNA release. Subsequently, a miniature air pump is activated to drive the DNA template through the pipetting channel, where a defined volume is quantitatively transferred into the detection chamber. The vibration motor is again engaged for 10 s to homogenize the solution in the detection chamber. The ceramic heater then maintains the detection chamber at 39 °C for 20 min to enable isothermal amplification. During this incubation, a 470 nm LED excites the fluorescent probe, while a photodiode equipped with a 525 nm bandpass filter collects fluorescence signals at 30-second intervals. The time threshold is automatically

determined and used to quantify *A. hydrophila* concentration based on a pre-established calibration curve.

2.9. Detection of target bacteria in the spiked aquaculture water

To evaluate the applicability of the portable microfluidic platform for detecting *A. hydrophila* in actual aquaculture environments, water samples were collected from aquaculture farms. After filtration and autoclave sterilization, the samples were spiked with *A. hydrophila* at concentrations ranging from 1×10^2–1×10^7 CFU·mL^{-1}. Each spiked sample was analyzed in triplicate using both the culture counting method and the developed microfluidic platform.

3. Results and discussion

3.1. Screening of primers

To minimize the risk of false-negative results due to potential nucleic acid contaminants, column-based purification was employed for DNA template preparation during primer screening. This approach ensured that the evaluation of amplification efficiency and specificity was not influenced by variables inherent in the sample processing. DNA templates were extracted from an *A. hydrophila* suspension (1×10^5 CFU·mL^{-1}) using a commercial bacterial genomic DNA extraction kit (DP302–02, Tiangen Biotech, China).

Three primer sets were randomly selected for negative control validation, with sterile double-distilled water (ddH_2O) used as template. As shown in Figs. 4A and 4B, no fluorescence signals were detected in any of the tested combinations, indicating the absence of primer-dimer formation or non-specific amplification. In subsequent comparative MIRA amplification experiments, conducted with equal DNA template concentrations, significant differences in amplification kinetics were observed among the primer sets. The F1-R1 primer pair consistently reached the fluorescence threshold more quickly (Figs. 4C and 4D), demonstrating superior amplification efficiency. This characteristic allows the F1-R1 pair to detect lower initial concentrations of *A. hydrophila*, thereby enhancing overall detection sensitivity. Based on these results, the F1-R1 primer pair was selected as the optimal set for all subsequent MIRA-based detection assays.

3.2. Optimization of nucleic acid extraction conditions

Systematic optimization of nucleic acid extraction parameters is crucial for obtaining DNA templates that support robust and sensitive MIRA detection. The rapid nucleic acid release reagent operates through a high-salt lysis mechanism, with extraction efficiency critically dependent on three key parameters: lysis temperature, lysis time, and bacterial suspension volume. To systematically identify the optimal extraction conditions, in-tube MIRA reactions monitored by a real-time PCR system were conducted.

To determine the optimal lysis temperature, 100 μL of *A. hydrophila* suspension (1×10^5 CFU·mL^{-1}) was lysed across a temperature gradient (25, 30, 35, 40, 45, 50, 55, and 60 °C) for 5 min. As shown in Fig. 5A, MIRA assay performance varied significantly with lysis temperature, with the most rapid amplification kinetics observed at 40 °C. This temperature represents a balance between two competing effects: enhanced cell wall disruption and DNA release at temperatures ranging from 25 to 40 °C, and thermally induced DNA degradation or co-precipitation of inhibitory substances in the high-salt buffer above 40 °C. The sensitivity of MIRA to inhibitors further amplified the detrimental impact of these precipitated contaminants.

To evaluate the effect of lysis time, standardized bacterial suspensions were lysed at 40 °C for various durations (3, 5, 7, 9, and 11 min). Statistical analysis revealed significant differences among the groups,

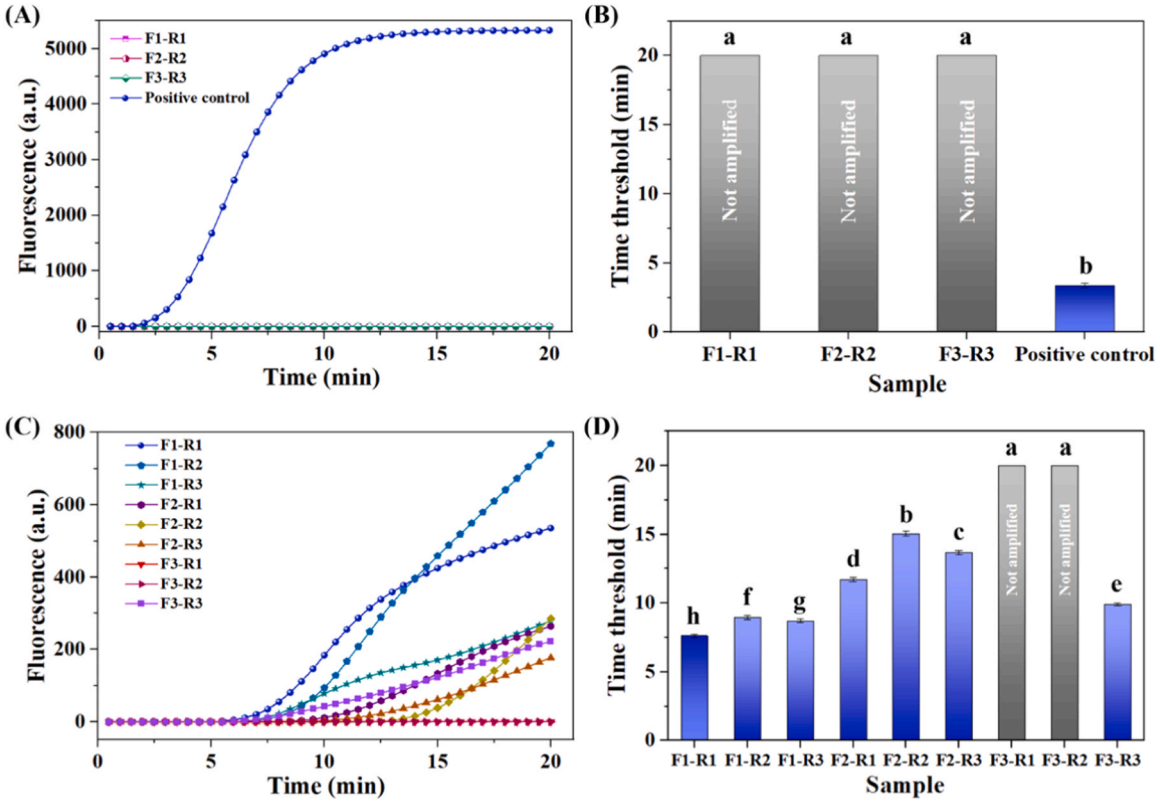

Fig. 4. Screening of the optimal primer combination for MIRA-based detection of *A. hydrophila*. (A, B) Specificity validation of primers and probe using sterile ddH_2O as the negative control (N = 3). (C, D) Evaluation of different primer combinations (N = 3). Statistical significance was determined by one-way ANOVA (n = 3, $P < 0.05$).

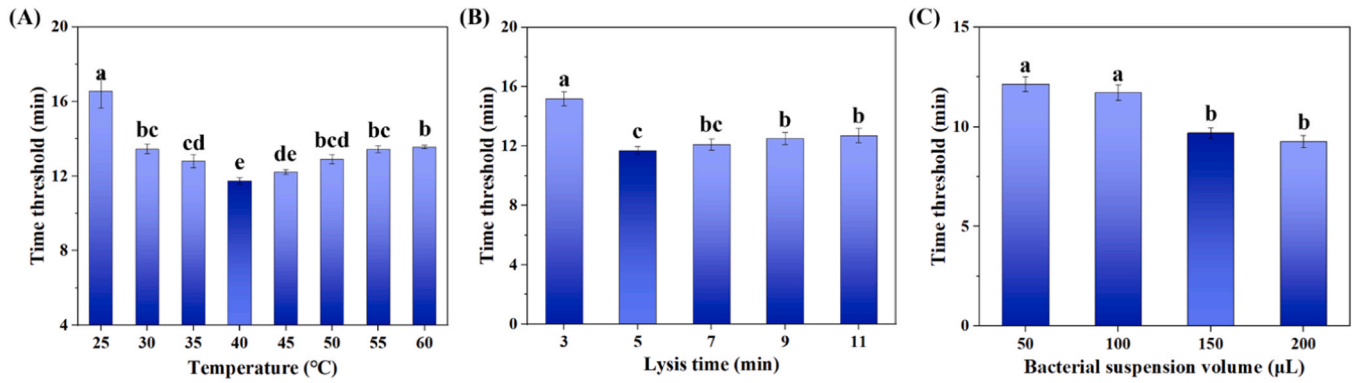

Fig. 5. Systematic optimization of nucleic acid extraction conditions. (A) Lysis temperature. DNA from *A. hydrophila* was obtained at different lysis temperatures across 25–60 °C for 5 min. (B) Lysis time. DNA was extracted at 40 °C over different lysis time from 3 to 11 min. (C) Bacterial suspension volume. DNA was extracted under optimal conditions from different volumes of bacterial suspension (50–200 μL). For all experiments, extracted DNA was analyzed using MIRA assay (N = 3). Statistical significance was determined by one-way ANOVA (n = 3, $P < 0.05$).

with 5 min yielding significantly better performance than both shorter and longer durations (Fig. 5B). Extending the lysis time from 3 to 5 min improved MIRA performance by promoting more complete cell lysis. However, further extension beyond 5 min likely caused DNA fragmentation under high-salt conditions and increased the release of inhibitors, ultimately reducing detection sensitivity.

Finally, nucleic acids were extracted from different bacterial suspension volumes (50, 100, 150, and 200 μL) under the optimized lysis conditions. MIRA results showed progressively higher amplification efficiency with increasing suspension volume, with 150 and 200 μL volumes performing significantly better than smaller volumes (Fig. 5C). This trend reflects the interplay between total DNA yield and inhibitor concentration. Considering both detection cost and chip size constraints, 150 μL was selected as the optimal suspension volume.

The high-salt lysis method streamlines nucleic acid extraction with enhanced simplicity and system compatibility compared to conventional physical (e.g., boiling, mechanical disruption), chemical (e.g., CTAB, SDS), or enzymatic (e.g., lysozyme, protease) approaches. It operates under mild conditions, avoiding high temperatures or harsh chemicals, yet effectively lyses bacterial cells and releases nucleic acids with minimal interference in downstream assays. Unlike enzymatic lysis, it does not require on expensive or labile enzymes, making it more suitable for pre-packaging and long-term storage in integrated microfluidic systems. This approach is particularly well-suited for low-biomass samples, such as aquaculture water and other environmental sources. In contrast, complex biological tissues rich in proteins and lipids, require additional purification using silica membranes or magnetic beads to remove inhibitors and improve nucleic acid purity [44,45]. These multi-step, centrifugation-dependent protocols, however, present challenges for full on-chip integration. Overall, the high-salt lysis method not only simplifies nucleic acid extraction but also improves compatibility with integrated detection platforms. Nevertheless, extraction strategies should be tailored to sample complexity and analytical requirements to balance efficiency, purity, and system integration [46].

3.3. Optimization of MIRA assay conditions

MIRA, a highly sensitive isothermal amplification technique, requires the optimization of several parameters, including reaction temperature, primer concentration, probe concentration, and DNA template volume, to achieve optimal performance. These parameters were systematically evaluated using in-tube reactions monitored by a real-time PCR system. DNA templates were extracted from *A. hydrophila* suspensions (1×10^5 CFU·mL^{-1}) under the established extraction conditions. The total reaction volume was adjusted to 50 μL with ddH_2O to accommodate variations in the volumes of the added components.

Temperature plays a critical role in MIRA by influencing enzymatic activity and overall reaction efficiency. When evaluated across a temperature gradient (37, 39, 41, 43, and 45 °C), notable differences in amplification performance were observed. The fastest fluorescence threshold attainment occurred at 39 °C (Fig. 6A), indicating optimal enzyme kinetics and amplification efficiency. This temperature strikes a balance between providing sufficient energy for nucleic acid strand separation and maintaining enzyme stability, thereby avoiding the progressive loss of activity seen at higher temperatures. Consequently, 39 °C was selected as the optimal reaction temperature.

Primer concentration is fundamental to amplification kinetics and specificity. Under the optimized temperature, different primer concentrations (0.2, 0.3, 0.4, 0.5, and 0.6 μM) were assessed, revealing clear differences in performance. The time threshold decreased as primer concentration rose from 0.2 to 0.4 μM, suggesting improved amplification efficiency due to greater primer availability. However, further increases to 0.5–0.6 μM did not substantially enhance performance, indicating that primer availability was no longer limiting beyond 0.4 μM (Fig. 6B). Given this saturation effect and the risk of non-specific amplification at high concentrations, 0.4 μM was chosen as the optimal primer concentration to ensure efficiency, specificity, and cost-effectiveness.

Probe concentration directly influences signal intensity and amplification efficiency. Evaluation of probe concentrations (0.08, 0.12, 0.16, and 0.2 μM) revealed performance differences across the tested range. Increasing the probe concentration from 0.08 to 0.16 μM reduced the time threshold, indicating more efficient hybridization and signal generation (Fig. 6C). However, at 0.2 μM, amplification time increased and background fluorescence intensified, suggesting that excess probes may compete with primers for target binding, thereby hindering amplification. Therefore, 0.12 μM was identified as the optimal probe concentration, balancing strong signal intensity with minimal background interference to achieve high sensitivity and detection accuracy.

DNA template volume is another key factor, as it modulates the availability of target sequences while potentially introducing inhibitors. Evaluation of different template volumes (3, 5, 7, 9, and 11 μL) revealed differences in amplification efficiency. The shortest time threshold was achieved with 5 μL of template (Fig. 6D). Although higher volumes (9–11 μL) showed slightly better efficiency than intermediate volumes, this may reflect a trade-off between increased target concentration and inhibitor carryover from the extraction process. The decline in efficiency at 7 μL suggests a dominant inhibitor effect in this range, whereas further volume increases might partially offset this by providing higher target availability. Due to its consistent performance and low risk of inhibition, 5 μL was chosen as the optimal template volume.

In summary, the systematic optimization of key parameters has

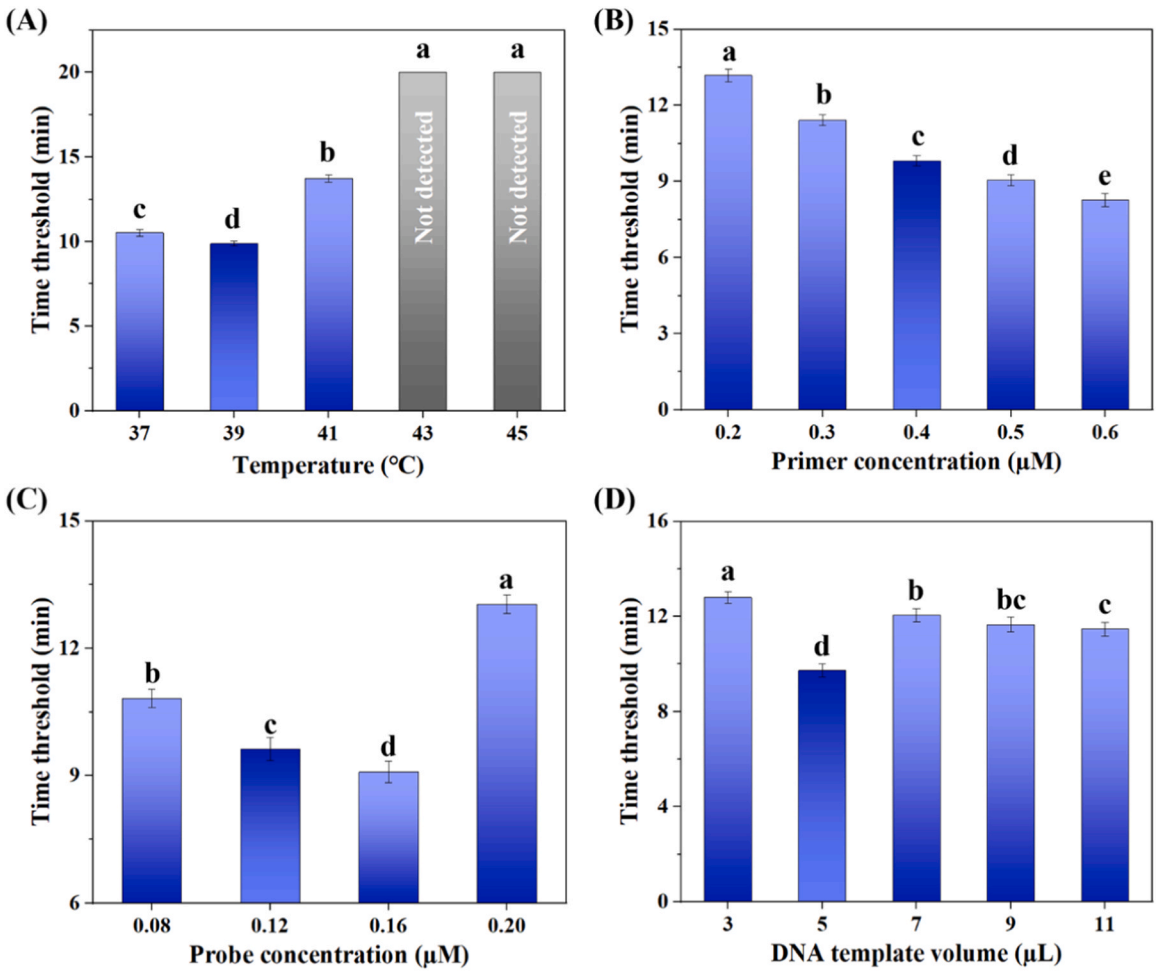

Fig. 6. Systematic optimization of MIRA reaction conditions. (A) Reaction temperature was tested across a range of 25–60 °C. (B) Primer concentrations were evaluated from 0.2 to 0.6 μM. (C) Probe concentrations were assessed from 0.08 to 0.2 μM. (D) DNA template volumes were analyzed from 3 to 11 μL. All MIRA reactions were performed in triplicate (N = 3). Statistical significance was determined by one-way ANOVA (n = 3, P < 0.05).

resulted in a robust and efficient MIRA assay protocol. The synergy among the optimized conditions enhances amplification speed, signal clarity, detection limit, and reproducibility. This refined methodology ensures consistent performance, which is essential for reliable on-site testing. Moreover, the structured optimization strategy introduced here is readily adaptable, offering a valuable template for developing MIRA-based detection systems for diverse bacterial and viral pathogens.

3.4. Validation of microfluidic chip surface modification

The efficacy of hydrophilic and hydrophobic surface modifications on PDMS microfluidic chips was evaluated through water contact angle measurements. The untreated PDMS surface exhibited a contact angle of 120.8° (Fig. 7A), consistent with its intrinsic hydrophobicity. Following hydrophilic modification, the contact angle sharply decreased to 11.2°

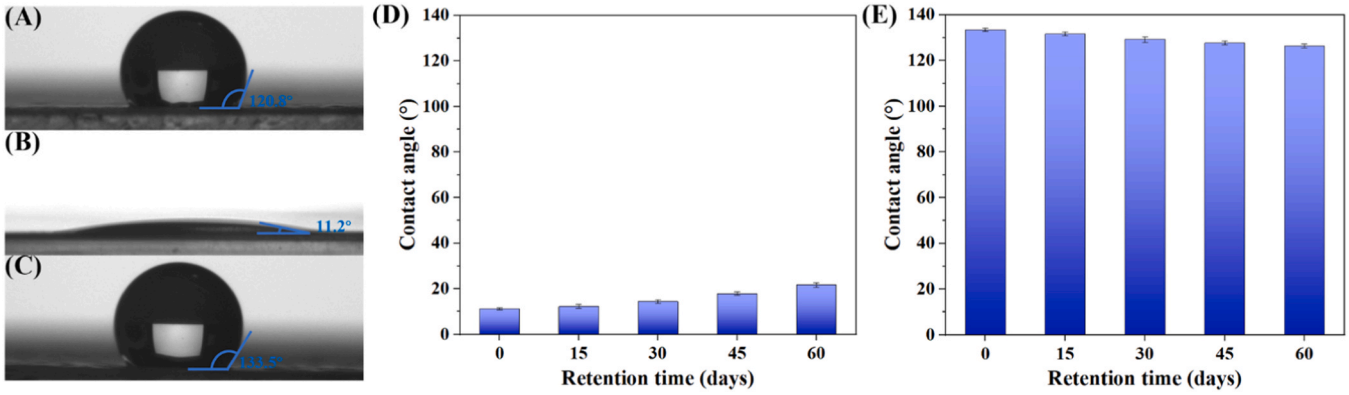

Fig. 7. Evaluation of surface modifications and their stability on the microfluidic chip. (A-C) Representative contact angles for the (A) untreated, (B) hydrophilic-, and (C) hydrophobic-modified surfaces. (D, E) Long-term stability of the (D) hydrophilic and (E) hydrophobic modifications, evaluated by contact angle measurements every 15 days during storage at 4 °C by vacuum (N = 3).

(Fig. 7B), indicating successful conversion into a highly wettable surface. In contrast, hydrophobic treatment increased the contact angle to 133.5° (Fig. 7C), further enhancing the inherent hydrophobic properties of the PDMS surface. Both modifications demonstrated excellent stability, maintaining consistent contact angles without significant changes when monitored at 15-day intervals over a 60-day period during vacuum storage at 4 °C (Figs. 7D and 7E). This confirms the long-term durability of the surface treatments.

The hydrophilic pipetting area ensures the quantitative transfer of DNA templates, while the hydrophobic reaction chambers and channels improve the chip's fluid propulsion capabilities. This modification strategy allows for precise internal liquid control by creating contrasting wettability in different functional zones, facilitating the development of fully automated microfluidic systems. The sustained contact angle stability over the 60-day storage period further underscores the remarkable durability of the surface modifications. This reliability ensures the mass production and long-term storage of pre-treated chips, significantly enhancing their practicality for field deployment.

3.5. Mixing efficiency of the vibratory mixer

Efficient reagent mixing within microfluidic chambers is essential for both nucleic acid extraction and MIRA amplification. Inspired by rubber pad-mediated vibration transmission for chamber mixing [47], we introduced circular perforations in the chip to embed miniature vibration motors. This design enables effective fluid mixing in both the extraction and detection chambers. To evaluate mixing performance, deionized water and blue dye were sequentially introduced into each chamber. After operating the motor for 10 s, complete mixing was visually confirmed (Fig. 8). For objective assessment, high-resolution images of the chambers were captured before and after mixing using a smartphone (HONOR 90 Pro, HONOR). The images were then converted to grayscale using ImageJ (NIH, USA), and the grayscale values along transverse lines were analyzed. The uniform grayscale distribution observed after mixing confirmed homogeneous mixing within 10 s (Fig. 8).

In contrast to passive mixing methods that rely on converging–diverging channel structures [48,49], this active mixing

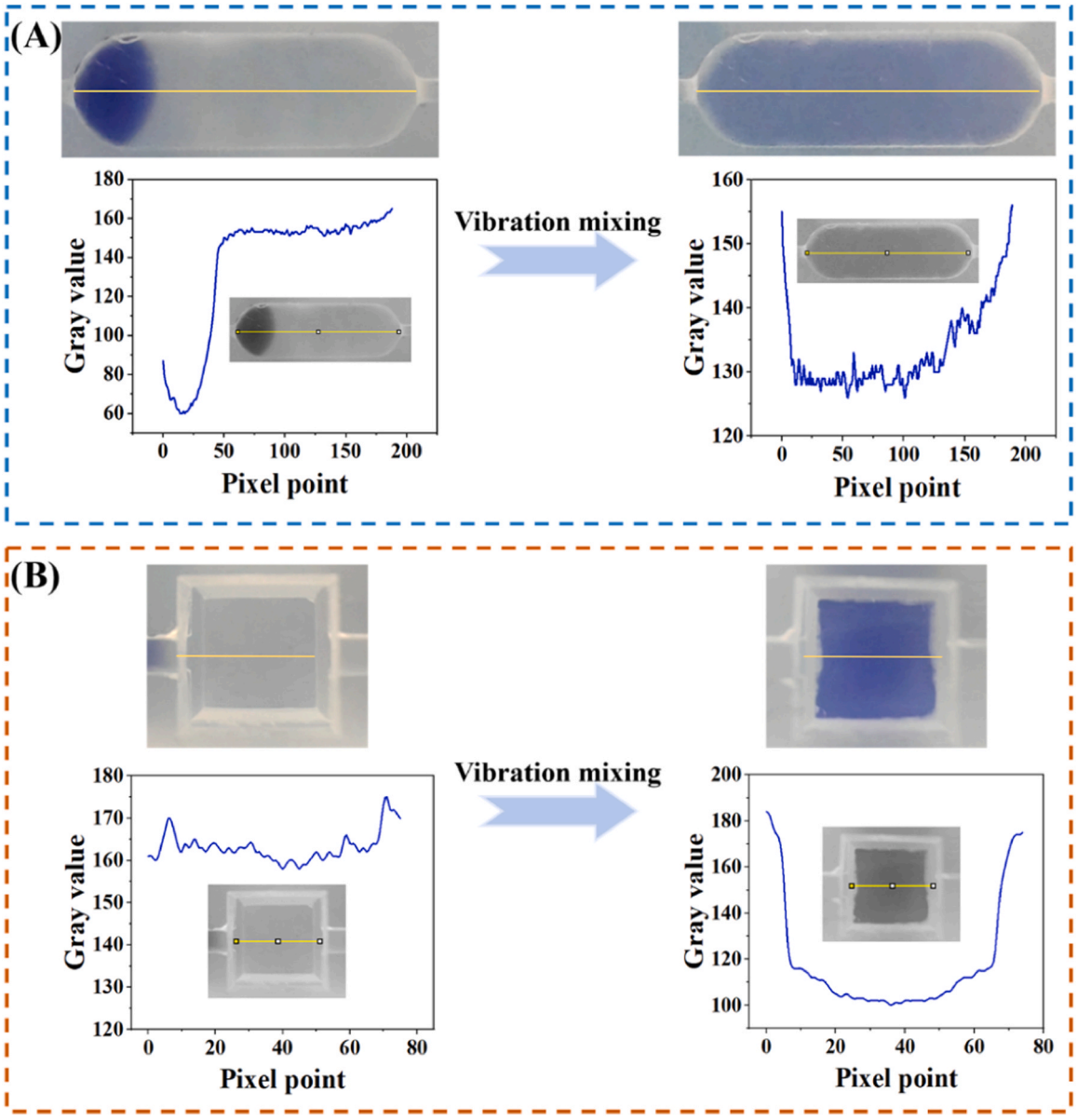

Fig. 8. Mixing efficiency of the vibratory mixer. (A, B) Visual assessment of mixing in the (A) nucleic acid extraction and (B) detection chambers before (left) and after (right) miniature vibration motor activation, demonstrating rapid and efficient homogenization.

strategy significantly improves homogenization efficiency and eliminates the need for complex channel designs. The embedded motor configuration allows simultaneous mixing in multiple chambers, enhancing resource utilization. Although the current mixing performance is robust, future studies should focus on elucidating the vibration transmission mechanism and optimizing the placement of excitation sources and chamber geometry to further improve reagent mixing efficiency.

3.6. Performance verification of single-threaded pipetting area

The performance of the single-threaded pipetting area is critical to the accuracy and sensitivity of downstream MIRA detection. To evaluate fluid dynamics within individual solution retention structures, we used COMSOL Multiphysics® (v6.2) to simulate the flow behavior. The simulations solved the incompressible Stokes equations and applied the Level Set method to track gas-liquid interface evolution. The results showed that air injection at 600 μL/min through the inlet effectively confined the aqueous solution within the retention zone, with excess fluid discharged through the outlet (Fig. 9A), confirming the designed working mechanism.

Experimental validation revealed that liquid surface tension significantly affected pipetting precision. To mitigate this effect, hydrophilic treatment was applied to the pipetting zones, and the air injection rate was systematically optimized. When 180 μL of deionized water was driven through the pipetting area at rates ranging from 100 to 500 μL/min, the volume transferred to the detection chamber was measured using a 0.1 mg-resolution balance (PX224ZH, OHAUS). The results showed clear differences in fluid retention across injection rates. Lower injection rates led to greater fluid retention in the pipetting area (Fig. 9B). At 100 μL/min, the transferred volume stabilized at 11.8 μL. Considering the previously optimized MIRA template volume of 5 μL (Section 3.3) and the trade-off between transfer volume and processing time, the bacterial suspension volume for nucleic acid extraction was set at 145 μL.

To evaluate manufacturing consistency, chips produced using different 3D-printed molds were tested by driving 174 μL of DNA template solution at 100 μL/min. The volume transferred to the detection chamber remained consistent at 5.34 μL (Fig. 9C), indicating reproducible performance across production batches. Additionally, the chip's pipetting accuracy was compared with a standard laboratory pipette (Eppendorf, 0.5–10 μL). Operators with basic training dispensed 5 μL of deionized water using the manual pipette, and volumes were measured using an analytical balance (three replicates per operator). The chip demonstrated accuracy comparable to manual pipetting (Fig. 9D), meeting all requirements for downstream applications.

Although this one-step pipetting operation simplifies the fluid control requirements of supporting equipment, the cascaded solution-retention structure increases the manufacturing complexity of the microfluidic chip. Nevertheless, chips fabricated with different 3D-printed molds exhibited highly consistent pipetting performance and accuracy on par with professional manual pipetting, providing a reliable

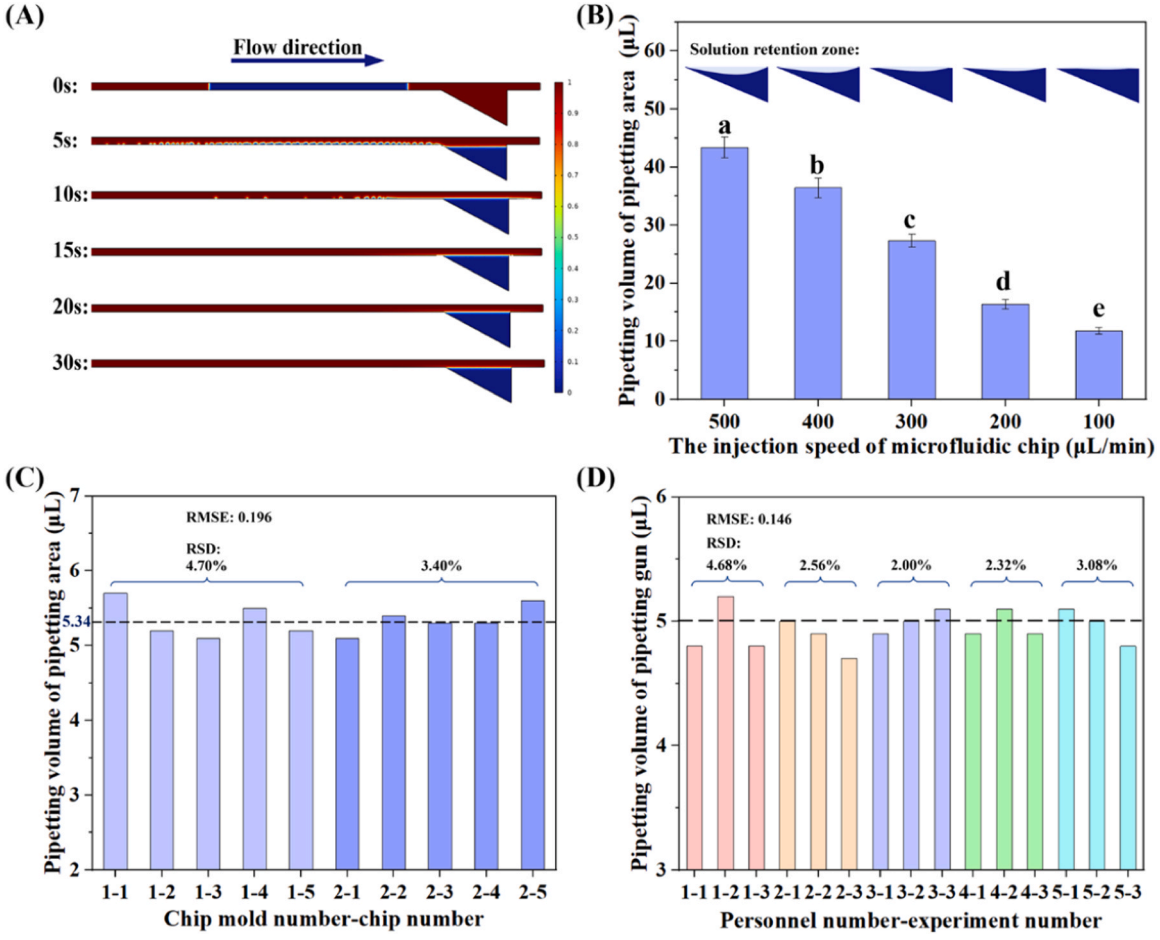

Fig. 9. Performance verification of the single-threaded pipetting area. (A) Simulation of gas-driven flow within the microchannel. (B) Operational performance across a range of injection speeds (100–500 μL/min) (N = 3). Statistical significance was determined by one-way ANOVA (n = 3, $P < 0.05$). (C) Consistency assessment across different chips (N = 3). Five chips from each of two fabrication molds were tested at a fixed flow rate of 100 μL/min. (D) Validation of pipette performance (N = 3). Pipetting performance was assessed by five trained operators. (RMSE: root mean square error).

technical platform for automated field detection. Future work will focus on optimizing the solution-retention architecture and integrating self-driven microfluidic technologies to further simplify pipetting operations.

3.7. Stability assessment of portable microfluidic platform

Accurate detection of *A. hydrophila* requires precise temperature control and reliable fluorescence monitoring. To overcome the limited heat transfer associated with substrate thickness in conventional bottom-heating setups, we integrated heating assemblies directly into the chip perforations. Each assembly includes ceramic heating pads connected to temperature sensors via thermally conductive electrical insulation (Fig. 10A), allowing independent thermal control of the nucleic acid extraction and detection chambers. As shown in Figs. 10B and 10C, thermocouple sensing junctions were placed at the geometric centers of the extraction and detection chambers to monitor temperature in real time. During the 100-second heating phase, both chambers maintained their set temperatures within a variation of ±0.2 °C, demonstrating excellent thermal stability throughout the process.

Reliable fluorescence detection is equally crucial for assay sensitivity. Repeated voltage measurements from the photodiode during detection of *A. hydrophila* (1×10^5 CFU·mL^{-1}) demonstrated highly consistent photodetector responses. The relative standard deviation (RSD) of signals measured at 5, 10, and 15 min of amplification remained below 4 % (Fig. 10D), confirming stable fluorescence monitoring throughout the amplification process.

Although this distributed heating method provides excellent thermal stability for individual chambers, it also introduces increased complexity in the temperature control system. Future work will explore alternative nucleic acid extraction methods, such as those using direct-current electric fields or ultrasonic lysis, to reduce dependency on precise temperature management and chemical reagents. In addition, the development of image-based fluorescence detection methods could significantly improve the platform's throughput and parallel processing capacity.

3.8. Performance of the portable microfluidic platform

Under optimal conditions, this portable microfluidic platform was used to detect *A. hydrophila* at concentrations ranging from 1×10^1–1×10^8 CFU·mL^{-1}. As shown in Fig. 11A, the threshold time decreased from 15.76 min to 6.53 min as the bacterial concentration increased from 1×10^2 to 1×10^7 CFU·mL^{-1}. A clear linear relationship was observed between the threshold time (*Tt*) and the logarithm of the target bacterial concentration (lgC_{Ah}), expressed as: $Tt = -1.7745 \lg(C_{Ah}) + 18.746$ ($R^2 = 0.9852$). The LOD of this platform was determined to be 10 CFU·mL^{-1}, defined as the lowest concentration that could be consistently and reliably detected [50,51], demonstrating excellent analytical performance. Furthermore, ten microfluidic chips were used to detect *A. hydrophila* at a concentration of 1×10^5 CFU·mL^{-1}. The detection results showed no significant differences among the chips,

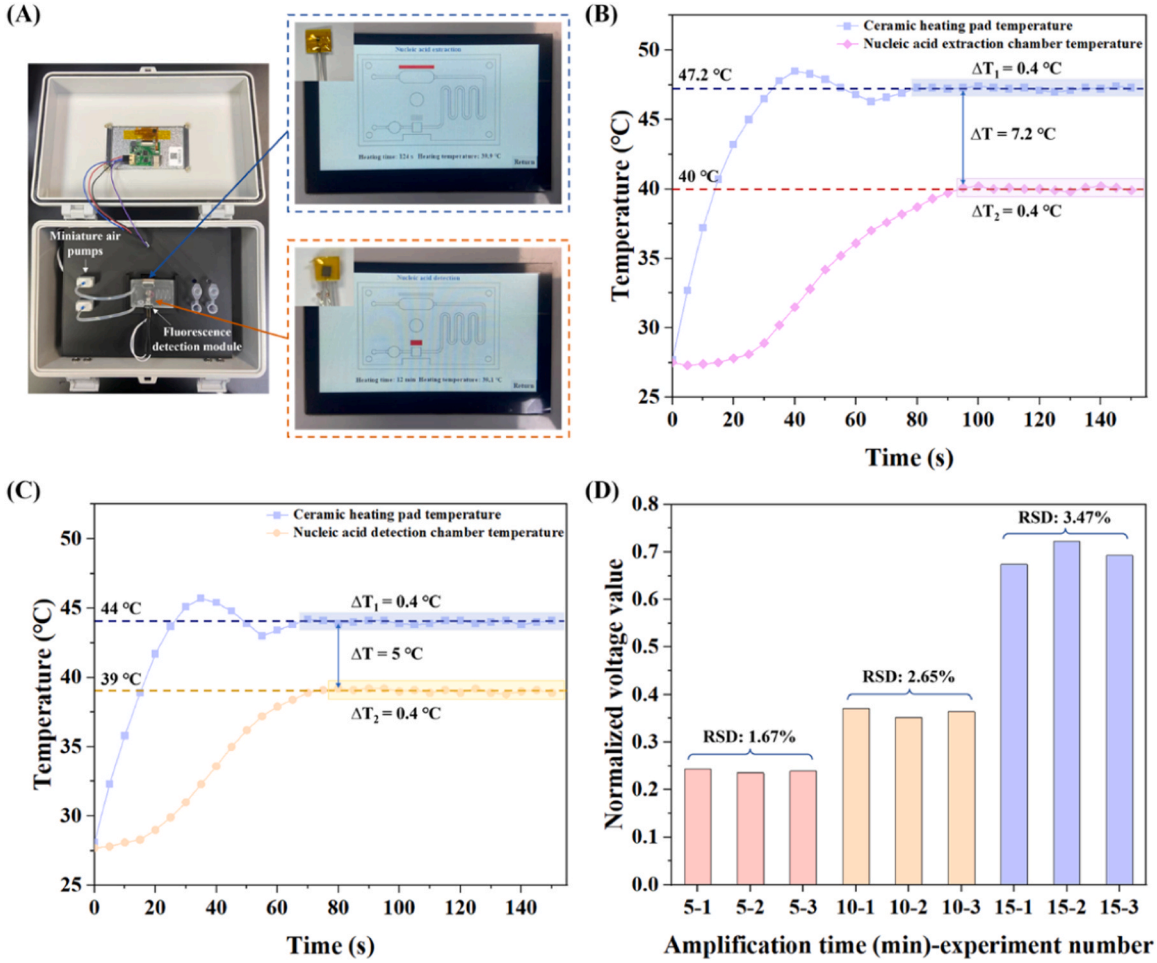

Fig. 10. Stability assessment of the portable microfluidic platform. (A) Photograph of the portable microfluidic platform. (B, C) Thermal performance of the nucleic acid extraction and detection chambers. Relationship between ceramic heating pad and chamber temperature. (D) Fluorescence detection stability (N = 3). Fluorescence intensity was measured at 5-minute intervals throughout the amplification process.

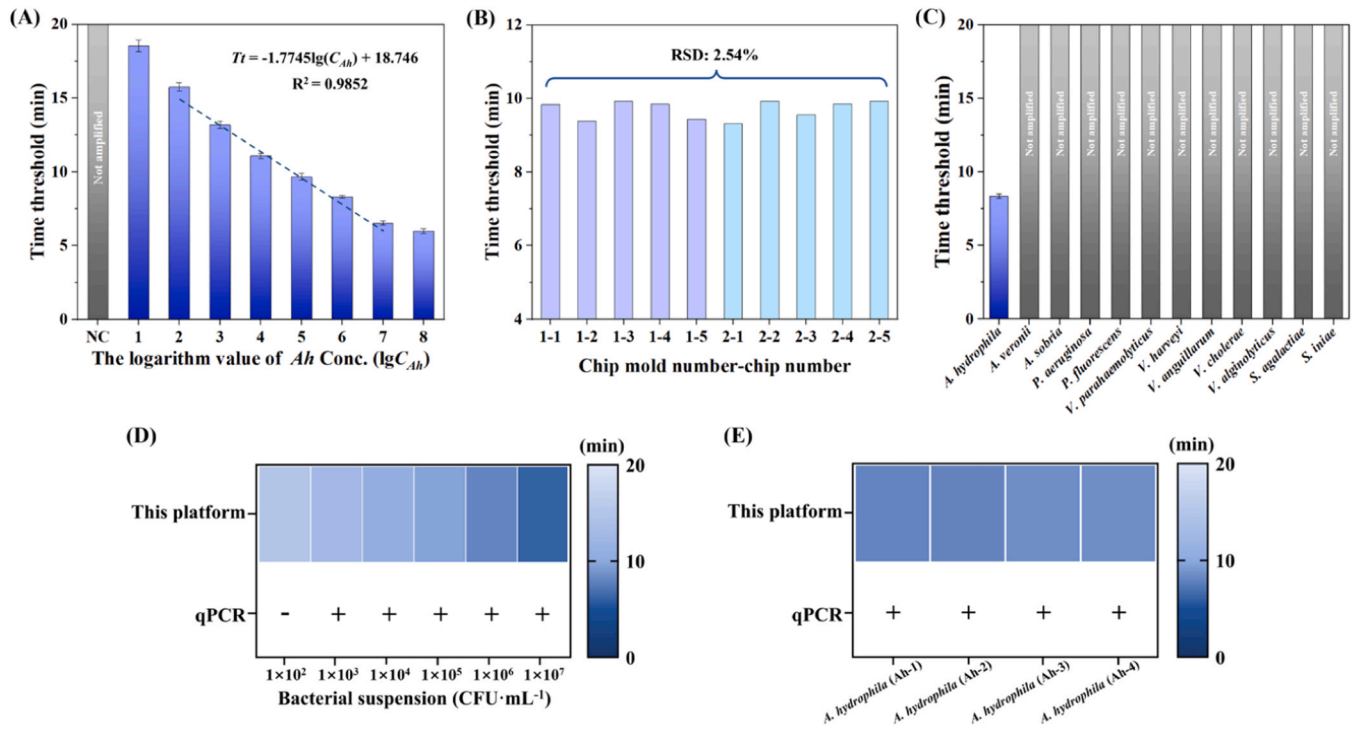

Fig. 11. Performance evaluation of the portable microfluidic platform. (A) Calibration curve for *A. hydrophila* detection (N = 3). A calibration curve was established by detecting *A. hydrophila* across a concentration range of 1×10^1–1×10^8 CFU·mL^{-1} under optimal conditions. (B) Chip-to-chip reproducibility assessment. The MIRA assay for *A. hydrophila* was performed on ten chips fabricated from each of two independent molds. (C) Specificity analysis (N = 3). The MIRA assay's specificity was validated against the target *A. hydrophila* and 11 non-target bacterial species. (D) Comparison with qPCR (N = 3). Both the platform and qPCR were used to detect *A. hydrophila* at various concentrations. (E) Detection of field-isolated strains (N = 3). Four field-isolated strains of *A. hydrophila* were detected using both the platform and qPCR.

with an RSD of 2.54 % (Fig. 11B). Variations between mold batches also had no significant impact on test results. These findings confirm that the platform exhibits excellent detection stability and repeatability.

Table S2 summarizes several previously reported detection methods for *A. hydrophila* with respect to LOD, linear range, and detection time. In comparison, the portable microfluidic platform offers equal or higher sensitivity, a shorter detection time, and a higher automation level. The enhanced performance can be attributed to the following factors: (1) primers targeting the *aerA* gene, enabling specific and efficient amplification; (2) a simple one-step pipetting process, ensuring highly consistent operation; (3) integration of efficient mixing and precise temperature control within the chip; and (4) automation of the detection process, minimizing errors associated with manual intervention.

3.9. Specificity and practicability of the portable microfluidic platform

The specificity of the portable microfluidic platform was evaluated using *A. hydrophila* (1×10^6 CFU·mL^{-1}) as the target bacterium, along with several non-target bacteria, including *A. veronii*, *A. sobria*, *P. aeruginosa*, *P. fluorescens*, *V. harveyi*, *V. parahaemolyticus*, *V. anguillarum*, *V. cholerae*, *V. alginolyticus*, *S. agalactiae*, and *S. phocae* (each at 1×10^6 CFU·mL^{-1}). As shown in Fig. 11C, only *A. hydrophila* yielded a positive signal, confirming the high specificity of the platform.

To assess the practicality of the platform, aquaculture water samples spiked with *A. hydrophila* at concentrations ranging from 1×10^2 to 1×10^7 CFU·mL^{-1} were analyzed using both the platform and qPCR. The platform demonstrated detection performance comparable to qPCR (Fig. 11D). In addition, recovery rates relative to the culture plate method ranged from 95.62 % to 119 %, with RSD values between 4.79 % and 8.97 % (Table 2), indicating reliable detection of *A. hydrophila* in aquaculture water. Further validation was conducted using field-isolated strains of *A. hydrophila* (Ah-1, Ah-2, Ah-3, and Ah-4) at 1×10^6 CFU·mL^{-1}. Both the platform and qPCR consistently produced positive signals for all strains (Fig. 11E), confirming the platform's robustness in detecting naturally occurring *A. hydrophila*. Although the per-test cost of the platform is higher than that of qPCR, the total system cost remains below $200 (Table S4 and S5). Given its low cost and the potential for broader applications, these results affirm the platform's suitability for on-site detection of *A. hydrophila* in aquaculture water.

Table 2
Detection of *A. hydrophila* at different concentrations in aquaculture water (N = 3).

Culture concentration (CFU·mL^{-1})	Detected concentration (CFU·mL^{-1})	Recovery (%)	RSD (%)
10^2	119	119.00	8.97
10^3	986	98.60	5.37
10^4	9562	95.62	6.28
10^5	99387	99.39	6.82
10^6	1068840	106.89	4.79
10^7	10497380	104.97	6.86

4. Conclusions

We have developed a portable microfluidic platform for the quantitative detection of *A. hydrophila* using MIRA technology. The platform autonomously performs nucleic acid extraction, precision pipetting, amplification, and detection, eliminating the need for laboratory instruments. Under optimized conditions, it achieved a detection range of 1×10^2 to 1×10^7 CFU·mL^{-1} for *A. hydrophila* within 40 min. Recovery rates for spiked aquaculture water samples at various concentrations ranged from 95.62 % to 119 %. The platform also demonstrated excellent performance in detecting field strains of *A. hydrophila*. With its

simple operation, high sensitivity, and rapid detection time, this platform holds significant potential for in-field screening of *A. hydrophila* in aquaculture water.

However, the lack of validation using aquaculture water samples with naturally occurring *A. hydrophila* infection remains a limitation of this study. This limitation is primarily due to the limited availability of such samples, which is influenced by seasonal variations, geographical location, and the sporadic nature of disease outbreaks. While the detection performance was evaluated in actual aquaculture water through spike-in experiments, further validation will be conducted once naturally infected samples become available.

Looking ahead, the platform's modular architecture will facilitate the development of a multiplex detection method targeting multiple virulence factors of *A. hydrophila*. This advancement is expected to expand the detection capability to include various pathogenic variants. Additionally, future efforts will focus on reducing detection costs by minimizing reaction volumes, implementing multiplexing, and utilizing bulk reagent formulations. These improvements will enhance the platform's applicability in resource-limited settings and support long-term, cost-effective use.

Environmental implication

Aeromonas hydrophila poses a significant environmental hazard in aquaculture, contaminating water bodies and causing disease outbreaks that threaten ecosystem health and sustainable production. Traditional pathogen detection methods are often lab-bound, slow, and impractical for on-site monitoring, delaying intervention and potentially enabling wider environmental contamination. This study presents a portable microfluidic platform enabling rapid (<40 min), sensitive (10 $CFU \cdot mL^{-1}$), and on-site detection directly in aquaculture water. Timely identification of such hazardous pathogens allows for immediate mitigation actions, preventing uncontrolled disease spread, reducing the need for prophylactic antimicrobials, and minimizing economic losses, thereby promoting more environmentally responsible and sustainable aquaculture management.

CRediT authorship contribution statement

Jie Han: Formal analysis. **Chen Li:** Methodology, Data curation. **Cong Wang:** Software, Formal analysis. **Tonglei Wu:** Methodology. **Yanying Zhang:** Methodology, Funding acquisition, Data curation. **Zhuangzhuang Bai:** Writing – original draft, Methodology, Formal analysis, Data curation, Conceptualization. **Daoliang Li:** Writing – review & editing, Supervision, Project administration, Funding acquisition, Formal analysis, Conceptualization. **Yan Zhang:** Writing – review & editing, Supervision, Project administration, Formal analysis, Conceptualization.

Declaration of Competing Interest

The authors declare that they have no known competing financial interests or personal relationships that could have appeared to influence the work reported in this paper.

Acknowledgements

This work was supported by the 2024-National Technology System for Shrimp and Crab Industry-Intelligent Farming (Grant no. CARS-48–28) and the Hebei Agriculture Research System+ (Grant no. HBCT2024280205).

Appendix A. Supporting information

Supplementary data associated with this article can be found in the online version at doi:10.1016/j.jhazmat.2025.140677.

Data Availability

The data that has been used is confidential.

References

[1] Verdegem, M., Buschmann, A.H., Latt, U.W., Dalsgaard, A.J.T., Lovatelli, A., 2023. The contribution of aquaculture systems to global aquaculture production. J World Aquacult Soc 54, 206–250. https://doi.org/10.1111/jwas.12963.

[2] Li, H., Cui, Z., Cui, H., Bai, Y., Yin, Z., Qu, K., 2023. Hazardous substances and their removal in recirculating aquaculture systems: A review. Aquaculture 569, 739399. https://doi.org/10.1016/j.aquaculture.2023.739399.

[3] Ceballos-Concha, A., Asche, F., Cárdenas-Retamal, R., 2024. Salmon aquaculture in Chile: Production growth and socioeconomic impacts. Rev Aquacult 17, e12993. https://doi.org/10.1111/raq.12993.

[4] Zhao, Y., Li, L., Yan, X., Wang, L., Ma, R., Qi, X., Wang, S., Mao, X., 2022. Emerging roles of the aptasensors as superior bioaffinity sensors for monitoring shellfish toxins in marine food chain. J Hazard Mater 421, 126690. https://doi.org/10.1016/j.jhazmat.2021.126690.

[5] Wright, A., Li, X., Yang, X., Soto, E., Gross, J., 2023. Disease prevention and mitigation in US finfish aquaculture: A review of current approaches and new strategies. Rev Aquacult 15, 1638–1653. https://doi.org/10.1111/raq.12807.

[6] Samsing, F., Barnes, A.C., 2024. The rise of the opportunists: What are the drivers of the increase in infectious diseases caused by environmental and commensal bacteria? Rev Aquacult 16, 1787–1797. https://doi.org/10.1111/raq.12922.

[7] Janda, J.M., Abbott, S.L., 2010. The genus *Aeromonas*: taxonomy, pathogenicity, and infection. Clin Microbiol Rev 23, 35–73. https://doi.org/10.1128/CMR.00039-09.

[8] Saharia, P.K., Hussain, I.A., Pokhrel, H., Kalita, B., Borah, G., Yasmin, R., 2021. Prevalence of Motile Aeromonas Septicaemia (MAS) in fish culture systems of the Central Brahmaputra Valley Zone of Assam, India. Aquacult Res 52, 1201–1214. https://doi.org/10.1111/are.14979.

[9] Nielsen, M.E., Hoi, L., Schmidt, A.S., Qian, D., Shimada, T., Shen, J.Y., Larsen, J.L., 2001. Is *Aeromonas hydrophila* the dominant motile Aeromonas species that causes disease outbreaks in aquaculture production in the Zhejiang Province of China? Dis Aquat Org 46, 23–29. https://doi.org/10.3354/dao046023.

[10] Li, F., Wu, D., Gu, H., Yin, M., Ge, H., Liu, X., Huang, J., Zhang, Y., Wang, Z., 2019. *Aeromonas hydrophila* and *Aeromonas veronii* cause motile Aeromonas septicaemia in the cultured Chinese sucker, *Myxocyprinus asiaticus*. Aquacult Res 50, 1515–1526. https://doi.org/10.1111/are.14028.

[11] Tartor, Y.H., EL-Naenaeey, E.Y., Abdallah, H.M., Samir, M., Yassen, M.M., Abdelwahab, A.M., 2021. Virulotyping and genetic diversity of *Aeromonas hydrophila* isolated from Nile tilapia (*Oreochromis niloticus*) in aquaculture farms in Egypt. Aquaculture 541, 736781. https://doi.org/10.1016/j.aquaculture.2021.736781.

[12] Hossain, M.J., Sun, D., McGarey, D.J., Wrenn, S., Alexander, L.M., Martino, M.E., Xing, Y., Terhune, J.S., Liles, M.R., 2014. An Asian origin of virulent *Aeromonas hydrophila* responsible for disease epidemics in United States-farmed catfish. mBio 5, e00848-14. https://doi.org/10.1128/mBio.00848-14.

[13] Haenen, O.L.M., Dong, H.T., Hoai, T.D., Crumlish, M., Karunasagar, I., Barkham, T., Chen, S.L., Zadoks, R., Kiermeier, A., Wang, B., Gamarro, E.G., Takeuchi, M., Azmai, M.N.A., Fouz, B., Pakingking, R., Wei, Z., Bondad-Reantaso, M.G., 2023. Bacterial diseases of tilapia, their zoonotic potential and risk of antimicrobial resistance. Rev Aquacult 15, 154–185. https://doi.org/10.1111/raq.12743.

[14] Zhou, H., Gai, C., Ye, G., An, J., Liu, K., Xu, L., Cao, H., 2019. *Aeromonas hydrophila*, an emerging causative agent of freshwater-farmed Whiteleg shrimp *Litopenaeus vannamei*. Microorganisms 7, 450. https://doi.org/10.3390/microorganisms7100450.

[15] Tang, J., Yang, X., Zheng, Z., Yu, W., Hu, K., Yu, H., 2006. Pharmacokinetics and the active metabolite of enrofloxacin in Chinese mitten-handed crab (*Eriocheir sinensis*). Aquaculture 260, 69–76. https://doi.org/10.1016/j.aquaculture.2006.05.036.

[16] Tao, Z., Xu, J., Dubey, S., Xu, C., Munang'andu, H.M., 2024. Infectious diseases of the Chinese soft-shelled turtle (*Pelodiscus sinensis*): A focus on etiological agents and predisposing factors. Aquacult Rep 37, 102227. https://doi.org/10.1016/j.aqrep.2024.102227.

[17] Semwal, A., Kumar, A., Kumar, N., 2023. A review on pathogenicity of *Aeromonas hydrophila* and their mitigation through medicinal herbs in aquaculture. Heliyon 9, e14088. https://doi.org/10.1016/j.heliyon.2023.e14088.

[18] Nhinh, D.T., Le, D.V., Van, K.V., Giang, N.T.H., Dang, L.T., Hoai, T.D., 2021. Prevalence, virulence gene distribution and alarming the multidrug resistance of *Aeromonas hydrophila* associated with disease outbreaks in freshwater aquaculture. AntibiotBasel 10, 532. https://doi.org/10.3390/antibiotics10050532.

[19] Zhang, D., Xu, D., Shoemaker, C., 2016. Experimental induction of motile Aeromonas septicemia in channel catfish (*Ictalurus punctatus*) by waterborne challenge with virulent *Aeromonas hydrophila*. Aquacult Rep 3, 18–23. https://doi.org/10.1016/j.aqrep.2015.11.003.

[20] Abdella, B., Shokrak, N.M., Abozahra, N.A., Elshamy, Y.M., Kadira, H.I., Mohamed, R.A., 2024. Aquaculture and *Aeromonas hydrophila*: a complex interplay of environmental factors and virulence. Aquacult Int 32, 7671–7681. https://doi.org/10.1007/s10499-024-01535-y.

[21] Pires, N.M.M., Dong, T., Yang, Z., da Silva, L.F.B.A., 2020. Recent methods and biosensors for foodborne pathogen detection in fish: progress and future prospects

to sustainable aquaculture systems. Crit Rev Food Sci Nutr 61, 1852–1876. https://doi.org/10.1080/10408398.2020.1767032.
[22] Tang, X., Zuo, J., Yang, C., Jiang, J., Zhang, Q., Ping, J., Li, P., 2023. Current trends in biosensors for biotoxins (mycotoxins, marine toxins, and bacterial food toxins): principles, application, and perspective. TrACTrends Anal Chem 165, 117144. https://doi.org/10.1016/j.trac.2023.117144.
[23] Bohara, K., Joshi, P., Acharya, K.P., Ramena, G., 2023. Emerging technologies revolutionising disease diagnosis and monitoring in aquatic animal health. Rev Aquacult 16, 836–854. https://doi.org/10.1111/raq.12870.
[24] Pilevar, M., Kim, K.T., Lee, W.H., 2021. Recent advances in biosensors for detecting viruses in water and wastewater. J Hazard Mater 410, 124656. https://doi.org/10.1016/j.jhazmat.2020.124656.
[25] Bai, Z., Xu, X., Wang, C., Wang, T., Sun, C., Liu, S., Li, D., 2022. A comprehensive review of detection methods for *Escherichia coli* O157:H7. TrACTrends Anal Chem 152, 116646. https://doi.org/10.1016/j.trac.2022.116646.
[26] Zhao, Y., Chen, F., Li, Q., Wang, L., Fan, C., 2015. Isothermal amplification of nucleic acids. Chem Rev 115, 12491–12545. https://doi.org/10.1021/acs.chemrev.5b00428.
[27] Luka, G., Samiei, E., Tasnim, N., Dalili, A., Najjaran, H., Hoorfar, M., 2022. Comprehensive review of conventional and state-of-the-art detection methods of *Cryptosporidium*. J Hazard Mater 421, 126714. https://doi.org/10.1016/j.jhazmat.2021.126714.
[28] Lu, Y., Li, M., Liu, H., Lin, S., Zhao, X., Liu, Z., Zhao, L., Wan, K., 2021. Detecting *Mycobacterium tuberculosis* complex and rifampicin resistance via a new rapid multienzyme isothermal point mutation assay. Anal Biochem 630, 114341. https://doi.org/10.1016/j.ab.2021.114341.
[29] Zhang, Y., Shao, F., Suo, F., Wang, Y., Wu, Q., Liu, T., Xie, Y., Gu, M., Fu, M., Li, S., Sun, X., 2025. Establishment and evaluation of rapid detection of AZFc deletion on Y chromosome based on multienzyme isothermal rapid amplification. Microchem J 208, 112556. https://doi.org/10.1016/j.microc.2024.112556.
[30] Petrucci, S., Costa, C., Broyles, D., Dikici, E., Daunert, S., Deo, S., 2021. On-site detection of food and waterborne bacteria – Current technologies, challenges, and future directions. Trends Food Sci Tech 115, 409–421. https://doi.org/10.1016/j.tifs.2021.06.054.
[31] Giuffrida, M.C., Spoto, G., 2017. Integration of isothermal amplification methods in microfluidic devices: Recent advances. Biosens Bioelectron 90, 174–186. https://doi.org/10.1016/j.bios.2016.11.045.
[32] Yin, W., Zhuang, J., Li, J., Xia, L., Hu, K., Yin, J., Mu, Y., 2023. Digital recombinase polymerase amplification, digital loop-mediated isothermal amplification, and digital CRISPR-Cas assisted assay: Current status, challenges, and perspectives. Small 19, 2303398. https://doi.org/10.1002/smll.202303398.
[33] Li, Z., Xu, X., Wang, D., Jiang, X., 2023. Recent advancements in nucleic acid detection with microfluidic chip for molecular diagnostics. TrACTrends Anal Chem 158, 116871. https://doi.org/10.1016/j.trac.2022.116871.
[34] Berlanda, S.F., Breitfeld, M., Dietsche, C.L., Dittrich, P.S., 2020. Recent advances in microfluidic technology for bioanalysis and diagnostics. Anal Chem 93, 311–331. https://doi.org/10.1021/acs.analchem.0c04366.
[35] Wang, X., Hong, X., Li, Y., Li, Y., Wang, J., Chen, P., Liu, B., 2022. Microfluidics-based strategies for molecular diagnostics of infectious diseases. Mil Med Res 9. https://doi.org/10.1186/s40779-022-00374-3.
[36] Han, X., Song, D., Xu, W., Lu, L., Zhu, A., Long, F., 2024. CRISPR/Cas12a powered air-displacement enhanced evanescent wave fluorescence fiber-embedded microfluidic biochip for nucleic acid amplification-free detection of *Escherichia coli* O157:H7. J Hazard Mater 469, 134037. https://doi.org/10.1016/j.jhazmat.2024.134037.
[37] Shu, B., Yang, J., Chen, W., Li, X., Xue, Y., Liu, M., Yin, X., Xu, L., Zhang, H., Qiu, J., Zheng, H., 2024. Temperature-programmed microfluidic CRISPR diagnostics enable rapid and automatous point-of-care testing for syphilis. Chem Eng J 496, 154174. https://doi.org/10.1016/j.cej.2024.154174.
[38] Wang, N., Zhang, Q., Liu, Y., Huang, B., Man, S., Ye, S., Ma, L., 2024. Sample-in-answer-out centrifugal microfluidic chip reaction biosensor powered by *Thermus thermophilus* Argonaute (*Tt*Ago) for rapid, highly sensitive and multiplexed molecular diagnostics of foodborne bacterial pathogens. Chem Eng J 495, 153434. https://doi.org/10.1016/j.cej.2024.153434.
[39] Li, Q., Duan, L., Jin, D., Chen, Y., Lou, Y., Zhou, Q., Xu, Z., Chen, F., Chen, H., Xu, G., Yan, M., Yang, G., Lu, J., Zhang, Y., Chen, J., 2024. A real-time fluorogenic recombinase polymerase amplification microfluidic chip (on-chip RPA) for multiple detection of pathogenic microorganisms of penaeid shrimp. Aquaculture 578, 740017. https://doi.org/10.1016/j.aquaculture.2023.740017.
[40] Shu, T., Yin, X., Xiong, Q., Hua, C., Bu, J., Yang, K., Zhao, J., Liu, Y., Zhu, L., Zhu, C., 2025. Lift-CM: An integrated lift-heater centrifugal microfluidic platform for point-of-care pathogen nucleic acid detection using isothermal amplification and CRISPR/Cas12a. Biosens Bioelectron 274, 117178. https://doi.org/10.1016/j.bios.2025.117178.
[41] Wang, S., Liu, N., Zheng, L., Cai, G., Lin, J., 2020. A lab-on-chip device for the sample-in-result-out detection of viable *Salmonella* using loop-mediated isothermal amplification and real-time turbidity monitoring. Lab Chip 20, 2296–2305. https://doi.org/10.1039/d0lc00290a.
[42] Huang, Y., Jiang, S., 2025. Quantification of viruses in wastewater on a centrifugal microfluidic disc. Environ Sci Technol 59, 3088–3097. https://doi.org/10.1021/acs.est.4c13718.
[43] Liao, J., Li, C., Liu, J., Cheng, H., Li, L., Tang, G., Huang, R., Lu, Y., Chen, S., Zhang, Q., Chen, H., Chen, Q., Chen, H., Sun, D., 2025. Automatic and integrated detection of nucleic acid by using a dual-mode thermal controlled digital microfluidic chip. Anal Chim Acta 1334, 343415. https://doi.org/10.1016/j.aca.2024.343415.
[44] Wang, S., Duan, H., Lin, J., 2023. A centrifugal microfluidic platform for rapid detection of pathogens based on chitosan nucleic acid extraction and RAA-T7-CRISPR/Cas13a nucleic acid detection. Sens Actuators B Chem 393, 134223. https://doi.org/10.1016/j.snb.2023.134223.
[45] Shen, F., Wei, J., Hui, Y., Quyang, L., Feng, H., Wu, L., Yu, X., Zhao, Z., Jin, Z., Zhou, W., 2025. High-transition-temperature paraffin integration in IFAST device for efficient and robust nucleic acid extraction and detection. Biosens Bioelectron 278, 117314. https://doi.org/10.1016/j.bios.2025.117314.
[46] Walden, C., Carbonero, F., Zhang, W., 2017. Assessing impacts of DNA extraction methods on next generation sequencing of water and wastewater samples. J Microbiol Methods 141, 10–16. https://doi.org/10.1016/j.mimet.2017.07.007.
[47] Qi, W., Zheng, L., Wang, S., Huang, F., Liu, Y., Jiang, H., Lin, J., 2021. A microfluidic biosensor for rapid and automatic detection of *Salmonella* using metal-organic framework and Raspberry Pi. Biosens Bioelectron 178, 113020. https://doi.org/10.1016/j.bios.2021.113020.
[48] Bai, Z., Wang, B., Gao, T., Xu, X., Du, Z., Han, J., Hu, Y., Bai, Y., Wang, L., Wang, C., Li, D., 2025. A novel microfluidic colorimetric biosensor for rapid and automatic detection *Escherichia coli* O157:H7 in aquaponics water. Comput Electron Agric 229, 109941. https://doi.org/10.1016/j.compag.2025.109941.
[49] Xue, L., Jin, N., Guo, R., Wang, S., Qi, W., Liu, Y., Li, Y., Lin, J., 2021. Microfluidic colorimetric biosensors based on MnO_2 nanozymes and convergence-divergence spiral micromixers for rapid and sensitive detection of *Salmonella*. ACS Sens 6, 2883–2892. https://doi.org/10.1021/acssensors.1c00292.
[50] Liu, L., Kasputis, T., Chen, J., Moore, M.D., Du, K., 2024. Fully integrated microfluidic digital chip for simple and highly quantitative detection of Norovirus. Anal Chem 96, 18408–18415. https://doi.org/10.1021/acs.analchem.4c03152.
[51] Yang, F., Wang, T., Wang, S., Li, M., Jia, K., Ding, Y., Lin, J., Xi, X., 2025. Cascaded gravity-driven microfluidic chip with tilt-actuated siphon valves for rapid detection of *Salmonella Typhimurium*. Anal Chem 97, 7231–7241. https://doi.org/10.1021/acs.analchem.4c06774.